

Original Article

A Novel Digital Phonocardiography Method to Identify the Cardiac Sounds through Intrinsic Time Scale Decomposition and Inter time space Measurement Between Cardiac Sounds

B. Sai Bharadwaj¹, Ch.Sumanth Kumar²

¹Department of Electronics & Communication Engineering, Vignan's Institute of Engineering for Women, Visakhapatnam, Andhra Pradesh, India,

²Department of Electrical, Electronics and Communications, GITAM Deemed to be University, Visakhapatnam, Andhrapradesh, India

¹Corresponding Author : research4816@gmail.com

Received: 11 October 2022

Revised: 21 November 2022

Accepted: 05 December 2022

Published: 25 December 2022

Abstract - The goal of this research is to create a dependable algorithm that checks the identification and categorisation of the first cardiac sound (S1) and the second cardiac sound (S2) of a phonocardiogram (PCG) signal in the presence of extracardiac sounds. The algorithm uses intrinsic time scale decomposition (ITD) integrated with Shannon energy (SE) to analyse cardiac sounds' existence and identification from the processed data. The algorithm's performance has been assessed with accuracy and computational time. This cardiac sound classification technique is used in medical diagnosis systems to investigate pathological heart states further. The proposed method can enhance the reliable identification of S1 and S2 cardiac sounds with the detection accuracy of 95.2% and 90.5% for S1 & S2, respectively.

Keywords - First cardiac sound, Second cardiac sound, Phonocardiogram, Intrinsic time scale decomposition, Shannon energy.

1. Introduction

According to the world health organisation, due to inapposite diagnostic services, an estimated 17.9 million deaths are caused by cardiovascular diseases [1]. The proper functioning of the heart generates the cardinal cardiac sounds S1 and S2 by the closure of the atrioventricular valve and semi-lunar valve, respectively [2]. These cardiac sounds can be auscultated and recorded with the help of a digital stethoscope [3]. Many cardiac abnormalities comprising valvular cardiac diseases, congestive cardiac failure and anatomical cardiac effects can be diagnosed with phonocardiography [4]. In the year 1819, French physician Rene Leanne invented the stethoscope [5]. The conventional stethoscope is an acoustic device that incorporates a diaphragm, and a hallow bell used to auscultate cardiac sounds. In a digital stethoscope, the cardiac sounds can be diagnosed with the diaphragm, which is further uprooted to another diaphragm inside the microphone; it leads to the conversion of acoustic sounds to electrical signals [6]. The cardiac sound components S1 and S2 and unusual sounds like murmurs, clicks, and snaps are recorded with the help of phonocardiography [7]. In a healthy cardiac cycle, the two major components are the S1 and S2 cardiac sounds if their association with other sounds indicates abnormalities in the heart [8, 9]. The first cardiac sound, S1(lub), has a

dull and prolonged characteristic with a longer duration (0.1 to 0.15s) and low pitch sound of frequency ranges from 10 to 200Hz. This cardiac sound can be auscultated at the arrival of the systolic phase [10]. The amplitude of the first cardiac sound, S1, has a significant positive correlation [11]. The second cardiac sound, S2(dub), has a short and sharp characteristic with a shorter duration of 0.08 to 0.12 seconds and a high pitch sound with a frequency range of 20-250Hz. This cardiac sound can be auscultated between the end of systolic and the arrival of diastolic phases [10]. The time duration from S2-S1 is longer compared to the duration from S1-S2 [29]. The third cardiac sound, S3, occurs just after the second cardiac sound (S2). The S3 sound has a soft and thudding quality of characteristics with a very low-frequency range from 25-70Hz, and its duration is 140-220ms. The fourth cardiac sound (S4) appears just ahead of S1 due to the ventricular expansion; vibrations are produced, which results in another abnormal cardiac sound [6]. This S4 cardiac sound has weak and rumbling characteristics with a frequency range of 15-70 Hz (lower than S3), and its duration is slightly before S1[10]. Traditional auscultation devices failed to distinguish S3 and S4 cardiac sounds [6], [10]-[12],[14]. Murmurs can occur due to an abnormal increase in blood flow through the cardiac structure, creating noise through damaged valves [15].



2. Literature Review

Normal cardiac sound segmentation involves two approaches, namely direct and indirect approaches. The direct method is based on ECG signal morphology as a reference in detecting the boundaries of cardiac sounds, whereas the indirect approach doesn't.

However, the study of Gharehbaghi [16] shows that direct heart sound segmentation requires extra hardware to provide an ECG signal. The segmentation is complex if the T-wave is too weak, thereby detecting the peaks and intervals localising S1 and S2 sounds. Mehak [17] have presented Shannon energy-based segmentation to classify the S1 and S2 cardiac sounds. Another work introduced by Ruman He [18] uses wavelet decomposition followed by Shannon energy computations for identifying the S1 and S2 components had given moderate accuracy. Noemi G and Marco K [19] have introduced a method that uses ECG signals as a reference to achieve good accuracy in classifying normal cardiac sounds. A performance study was carried out by Choi S [20] on these methods and presented that the Shannon energy method performed better than the Hilbert envelope method under noisy conditions. Moukadem A [13] has developed a robust segmentation method based on the S transform.

However, the S transform has failed to detect the boundaries for weak components as it suffers from low energy concentration in the time domain. A minimum complexity is observed in Empirical mode decomposition (EMD), which decomposed the given PCG signal into certain functions known as Intrinsic mode functions (IMFs) [22]. Another popular method, Hilbert vibration decomposition (HVD), introduced by Feldman, makes a signal to decompose iteratively. At a given iteration, a slowly varying component appears as a residue with lower energy concentration levels [23]. The crucial step in decomposition is identifying the limits for low pass action to produce slow varying components. Other methods in analysing the cardiac sounds include the Short-time Fourier transform (STFT), presented by P.S.Vikhe et al. [24] and calculated the transition time and frequency contents of S1 and S2. Finding the solutions to the above two issues can reinforce the accuracy of the detection of cardiac sounds. This work presents a novel approach mentioned at the higher side in detecting S1 and S2 based on ITD [25], which does not consider ECG signals as a reference. Shannon energy is calculated further on the decomposed components to localise the cardiac sounds S1 and S2.

The upcoming sections of this paper are organised as follows. Section 3 gives a brief outline of the proposed system and its workflow. Section 4 discusses the methods. Section 5 provides the results, and localisation rules for S1 and S2 identification are continued in section 6. Conclusions are given in section 7.

3. System Overview

A speculative approach to detecting first and second cardiac sounds is introduced, followed by a key procedure

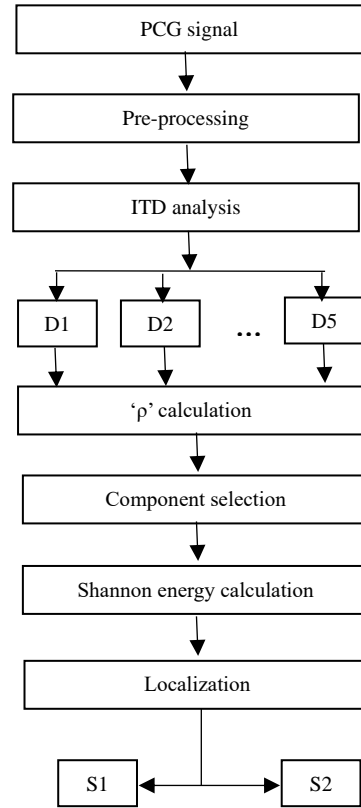


Fig. 1 Proposed Workflow

described in Fig.1. Firstly, the input PCG signal is filtered to make it noise-free. Then the ITD method is applied to decompose into l number of components. The reliable number of components depends on the correlation factor (ρ). Firstly, the input PCG signal is filtered to make it noise-free, and then the ITD method is applied to decompose it into l number of components.

The reliable number of components depends on the correlation factor (ρ). This work $l = 5$ provides a comparative result for further processing. A proper component selection is made on which Shannon energy is computed, followed by thresholding. Finally, the exact locations of S1 and S2 sounds are determined by the criteria described in section 5.

4. Proposed Method

4.1. Intrinsic Time Scale Decomposition

The primary purpose of the intrinsic time scale decomposition technique is to decompose a signal into a sum of proper rotation components and a baseline signal (monotonic trend) with a well-defined frequency and amplitude. The baseline signal (L_t) and proper rotation residuals (H_t) are low and high-frequency component signals. The input signal U_t can be decomposed as the sum of the baseline and proper rotational signal.

$$U_t = \mathcal{L}U_t + (1 - \mathcal{L})U_t = L_t + H_t \quad (1)$$

If U_t be a real-valued causal signal, and the local extrema of U_t can be denoted with τ_i where $i=1, 2, 3...$ In case U_t is constant for a particular interval, it contains local extrema as its right endpoint of the interval due to adjacent signal fluctuations. We can define the baseline extracting operator' \mathcal{L} ' on the interval $(\tau_i, \tau_{i+1}]$ between two successive extremes. α is the gain control constant and L_{i+1} is the node of the baseline signal, which is calculated from (2).

$$L_{i+1} = \alpha \left[U_i + \frac{(\tau_{i+1} - \tau_i)}{(\tau_{i+2} - \tau_i)} (U_{i+2} - U_i) \right] + (1 - \alpha) U_{i+1} \quad (2)$$

$$\mathcal{L}U_t = L_t = L_{i+1} + \left[\frac{(L_{i+1} - L_i)(U_t - U_i)}{(U_{i+1} - U_i)} \right], t \in (\tau_i, \tau_{i+1}) \quad (3)$$

Where baseline signal (U_t) and proper rotation residual (H_t) have been defined on $[0, \tau_i]$ and U_t is defined for $t \in [0, \tau_{i+2}]$. The value of α ranges from (0, 1) but is generally fixed as $\alpha=1/2$. In this manner, we can obtain the baseline signal (L_t). To make U_t monotonic between extremes, the baseline signal L_t should be a linear transformation of the original signal. With the help of nodes obtained, the baseline signal is reconstructed. After obtaining the baseline signal, the proper rotation residual is obtained by (1).

4.2. Shannon Energy

The third-order Shannon energy (TOSE) is used here for PCG signal envelope detection. As noticed from [26], Wang et al. used TOSE for PCG segmentation and showed that it attenuated unwanted low-intensity components. The average TOSE is calculated as follows

$$E = -\frac{1}{L} \sum_{i=1}^L |U(i)|^3 \log |U(i)|^3 \quad (4)$$

Where, L is the number of samples in that segment. Then the normalisation gives an effective amplification for high and medium-intensity components. The presence of low-intensity components in a PCG signal is due to murmurs, speech and ambient noise, leading to incorrect segmentation of cardiac sounds.

5. Results and Discussions

A PCG acquisition device-associated amplifier circuit was designed to capture and amplify the signals to validate the suggested method's performance. The PCG capture is made possible by a specially built-microphone probe. The microphone sensor is made up of a condenser microphone as well as the related electrical circuitry. It is housed in a sealed container shaped like a little cone, identical to a traditional stethoscope. Because the microphone probe's frequency response runs from 2Hz to 250Hz, it is suitable for capturing PCG signals for analysing the two main heart sounds, whose center frequency varies from 20Hz to 200Hz. The mic sensor's placement across the patient's chest is unconventional since ideal auscultation sites for heart sounds differ depending on the subject.

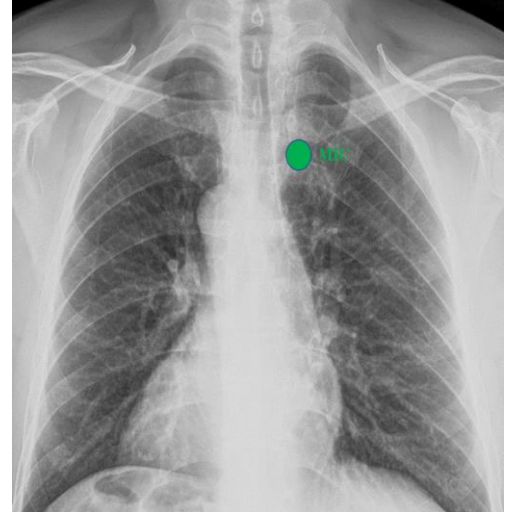


Fig. 2 Approximate arrangement of the microphone sensor for PCG signal collection

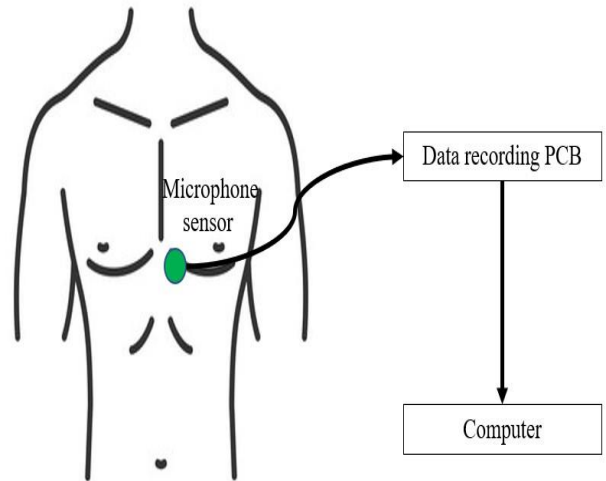


Fig. 3 Block schematic for experiment hardware setup

As a result, the examiner must trial to locate a location that provides a high-quality PCG signal. Fig.2 depicts the conventional location of the microphone sensor on the patient's chest. While seeing the signal on the host machine, the search for the correct spot is carried out. Data were gathered from 14 healthy participants. The microphone output is routed to a data recording PCB, which contains an instrumentation amplifier and a bandpass filter with a gain of 2 implemented with an operational amplifier. Fig.3 depicts the hardware design for physically gathering and analysing the PCG data.

Along with the manual acquisition, a good range of cardiac sound data is chosen from the University of Michigan's heart sound database [27] and the department of Washington database [28]. 7 PCG signals with S3 and S4 counts were chosen for proper analysis to test the proposed algorithm. A total of 24 acquired signals were sent into a computer and investigated using Matlab simulation. These cardiac sound signals are recorded at 44.1 kHz.

5.1. Preprocessing

The first step in the proposed workflow seems to be to pre-process the signal. Denoising and normalising the raw signal are two phases in pre-processing. Because it incorporates a succession of high and low pass filters, the discrete wavelet transform method is employed for efficient denoising [8]-[10]. The resulting signal is normalised, so all signals have the same amplitude ranges. If $U(t)$ is the original input to be processed, then $U_{norm}(t)$ represents its normalised value.

$$U_{norm}(t) = \frac{U(t)}{R} \quad (5)$$

Where $R = \text{maximum}(U(t))$, the obtained signal is passed further through a low pass filter with a cut-off frequency 200Hz, as the first cardiac sound(S1) has a frequency less than 200Hz.

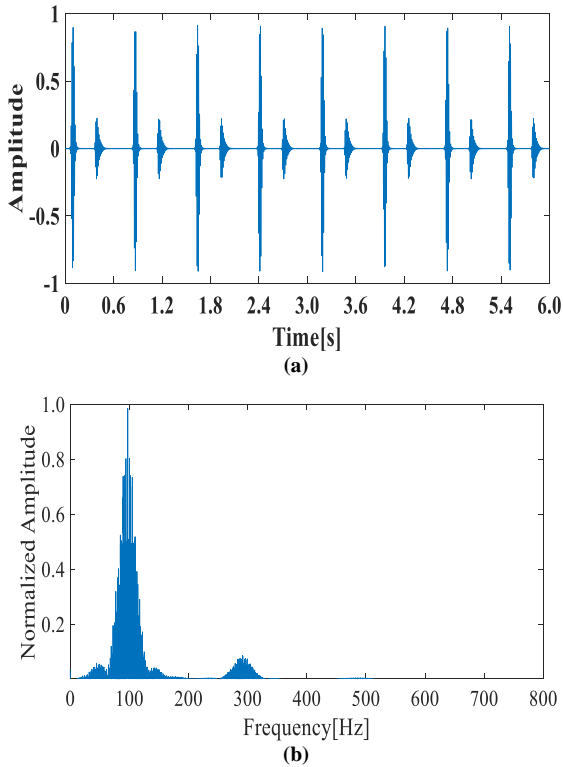


Fig. 4 (a) Input PCG signal (b) FFT of the input PCG Signal

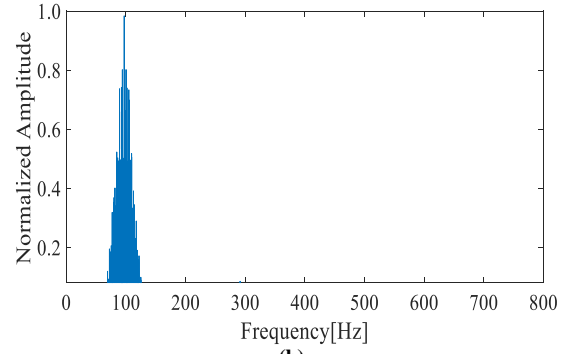
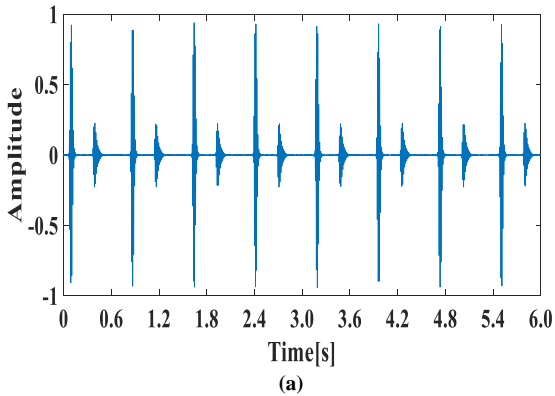


Fig. 5 (a) Filtered PCG signal output (b) FFT of filtered PCG signal

The input signal and its FFT output are shown in Fig.4, consisting of primary and secondary components. A secondary component is observed due to noise present in the input cardiac sound signal. The filtered output and the FFT of the filtered signal are shown in Fig.5, where it contains only the primary component.

The filtered and normalised output of the PCG signal is given to the decomposition block for further analysis.

5.2. Decomposition

A robust decomposition algorithm introduced by Frei and Osorio[26] allows the PCG signal to decompose into a baseline and a proper rotation component at every iteration.

The noise-free PCG signal is allowed to decompose using the ITD approach into five levels (D1, D2, D3, D4, and D5). Out of five successive decomposed levels, the first three decomposed levels are considered and presented in Fig.6 as they showed dominance comparatively with other levels.

5.3. Component Selection

In each level of decomposition, a baseline component was observed for analysis. A significant decomposed component at a particular level is confirmed by calculating the Root mean square deviation (RMSD) and correlation factor (ρ) between original and decomposed signals. The RMSD is calculated as

$$RMSD = \sqrt{\frac{\sum_{k=1}^K |D(k) - A(k)|^2}{K}} \quad (6)$$

Where $A(k)$ and $D(k)$ are actual and reconstructed signals, where k refers to the data sample index and K is the total number of sampled data. For each level of decomposition, ρ and RMSD are calculated, and Fig 7 shows the plot of ρ and RMSD for all five decomposition levels.

From Fig.7, the component obtained in D2 exhibited high correlation than other levels of decomposition, and it was considered for further processing. It was found that $\rho = 0.95$ for level 2 decomposed showed a minimum error and good correlation.

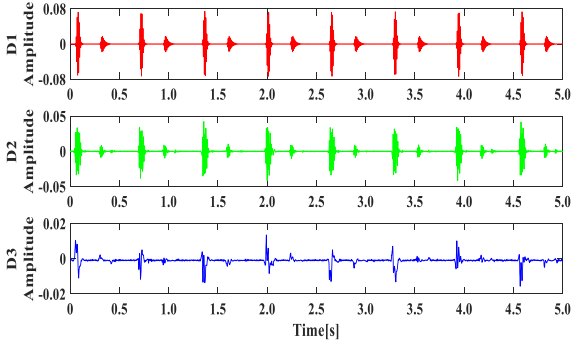
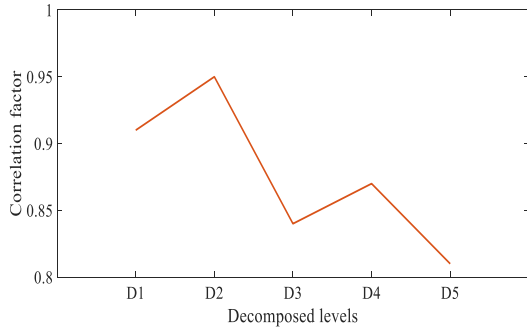
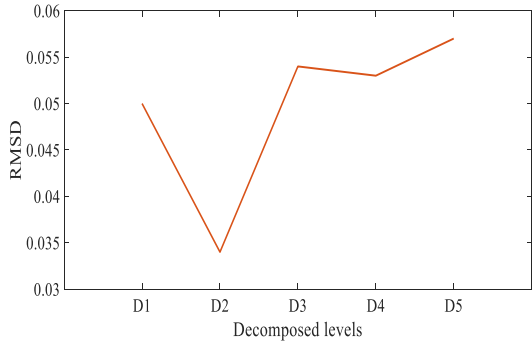


Fig. 6 Decomposition levels of ITD



(a)



(b)

Fig. 7 (a) Plot of Correlation values and (b) RMSD values for five levels of decomposition

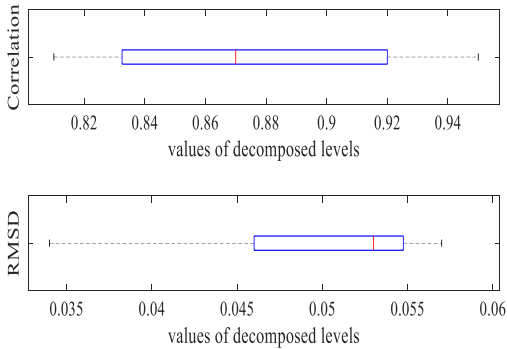


Fig. 8 Variations of correlation and RMSD values

The error margin of the correlation factor is $0.876 \pm 4.97\%$ and $0.0496 \pm 14.3\%$ for RMSD. The same is plotted in Fig.8. Third-order Shannon energy is applied to the selected D2 component to enhance higher and medium

energy components. Thereby it increases the identification probability of S1 and S2.

5.4. Shannon Energy Calculation

The average TOSE obtained from (4) is used for further computing. Then the normalised average TOSE is computed from (7).

$$E_{\text{Norm}} = \frac{E - E_{\mu}}{E_{\sigma}} \quad (7)$$

Here E_{μ} is the mean value of E and E_{σ} is the standard deviation of E . In order to isolate the required components from other sounds, an adaptive energy threshold (ETR) is applied and calculated as follows

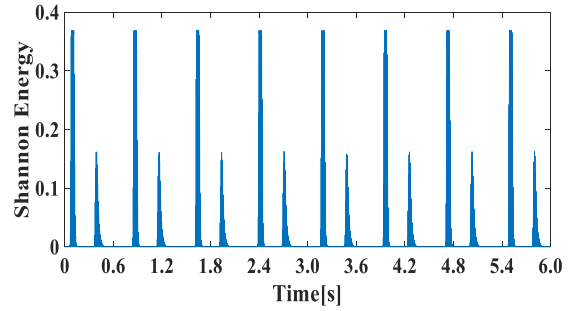


Fig. 9 Shannon energy plot of D2

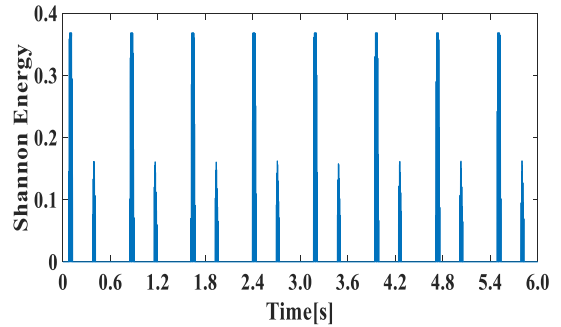


Fig. 10 Shannon energy plot of D2 after thresholding

$$ETR = \frac{1}{m} \sum_{i=1}^m E_{\text{Norm}}(i) \quad (8)$$

Where $E_{\text{Norm}}(i)$ is obtained from the (7) calculated periodically to establish ETR. Fig.9 and Fig.10 depict the observable peaks in the Shannon energy plot. Dynamic thresholding is applied to the Shannon energy plot to find the location of the cardiac sounds.

6. Localisation

6.1. Locating S1 and S2

Finally, the detection rules are implemented to determine the exact locations of S1 and S2. The detection rules are based on calculating the time distance index (TDI). TDI measures the intertimespace between the adjacent peaks. Table 1 presents the TDI measurements for the recorded PCG signals from 13 individuals.

Table 1. TDI measurements and observations for recorded signals

ID	Gender	Age	BPM	TDI (ms)	Observations
Participant_01	M	27	77	486	S1 & S2 are detected properly
Participant_02	F	20	72	475	S1 & S2 are detected properly
Participant_03	F	21	67	471	S1 & S2 are detected properly
Participant_04	F	21	69	487	S1 & S2 are detected properly
Participant_05	M	33	70	471	S1 & S2 are detected properly
Participant_06	F	41	75	491	S1 & S2 are detected properly
Participant_07	M	42	69	477	S1 & S2 are not appropriately detected due to interfering components
Participant_08	M	39	79	482	S1 & S2 are detected properly
Participant_09	M	18	76	483	S1 & S2 are detected properly
Participant_10	M	22	72	488	S1 & S2 are detected properly
Participant_11	M	21	67	479	S1 & S2 are detected properly
Participant_12	M	21	70	480	S1 & S2 are detected properly
Participant_13	F	20	69	477	S1 & S2 are detected properly
Participant_14	F	20	79	481	S1 is detected properly
Participant_15	F	21	79	488	S1 & S2 are detected properly

6.2. Locating S1 and S2 in S3 or S4 Presence

The abnormal activity of the heart results in extracardiac sounds (S3 and S4). This special case has investigated the signals where odd components' energy is deficient compared with normal features. If the input signal consists of first, second and third cardiac sounds (S1, S2 and S3), as presented in Fig.11 (a). From Fig.11 (b), considering the above rules, the lowest energy peak, S3, gets neglected as the time distance between S2 and S3 is in the range of 140ms to 220ms.

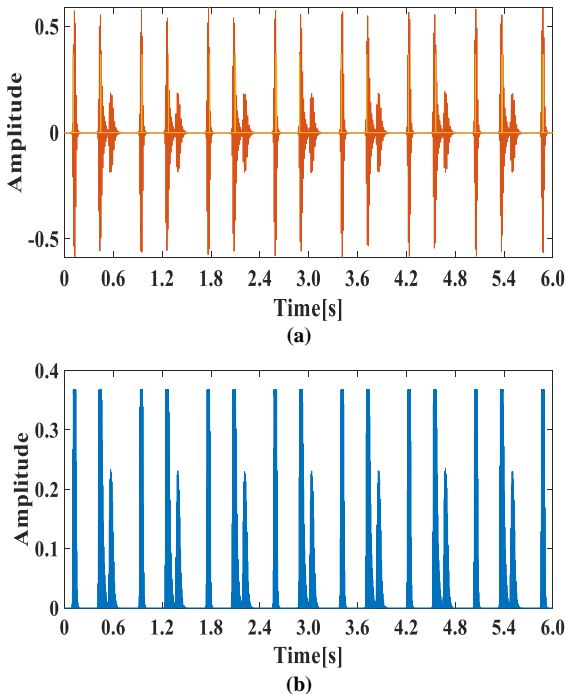


Fig. 11 (a) PCG signal plot consists of S1, S2 and S3 (b) Shannon Energy plot after thresholding

Consider another input PCG signal that contains the first and second cardiac sounds along with abnormal cardiac sound S4 is shown in Fig.12 (a). The SE plot of the signal is observed in Fig.12 (b). As same as in the S3 case,

S4 should be discarded, and S1 and S2 are correctly identified. The abnormal sound S4 should be discarded to identify S1 and S2 cardiac sounds correctly.

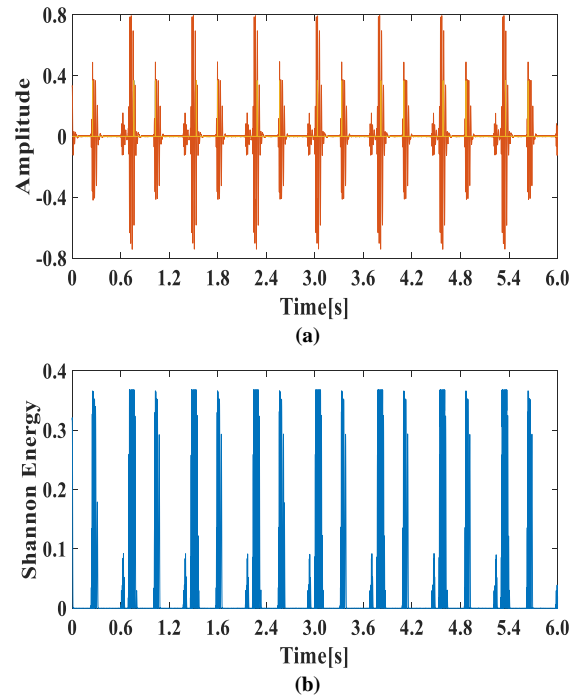


Fig. 12 (a) PCG signal with S1, S2 and S4 (b) Plot of Shannon Energy after thresholding

Table 2 presents the TDI measurements for the recorded PCG signals from 13 individuals. The performance of the proposed method evaluates with the parameter accuracy (Acc). The accuracy defined in (9) tells the method's efficiency in detecting normal cardiac sounds.

$$Acc = \frac{\text{number of S1s or S2s identified}}{\text{Total number of cardiac cycles}} \times 100 \% \quad (9)$$

Table 2. TDI measurements and observations for collected signals from databases

ID	Signal description	TDI (ms)	Observations
Signal_01	PCG signal with S3	488	S1 & S2 are detected properly
Signal_02	PCG signal with S4	478	S1 & S2 are detected properly
Signal_03	PCG signal with S3	479	S1 & S2 are detected properly
Signal_04	PCG signal with S3 and Holosystolic Murmur	487	S1 & S2 are detected properly
Signal_05	PCG signal with S4	481	S1 & S2 are detected properly
Signal_06	PCG signal with S4 and Mid-Systolic Murmur	491	S1 is detected properly

As this work considered, 21 PCG signals were identified with 108 cardiac cycles. The accuracy in the detection of S1 and S2 is limited by noise and additional cardiac sounds. For some subjects, the cardiac cycles are not maintained in the specified time intervals may lead to wrong interpretation.

Table 3. Accuracy comparison with other methods

Methods	S1 Acc (%)	S2 Acc (%)
EMD [23]	92.8	86.4
HVD [24]	85.1	80.7
STFT [25]	90.4	85.1
Proposed	95.2	90.5

The calculated accuracy for the proposed and existing methods listed in Table 3 demonstrates that the proposed method attained a higher accuracy than other methods. The number of S1s, S2s or the number of cardiac cycles is calculated on visual perception only. In the process of identification of cardiac sounds, the efficiency of the

References

- [1] [Online]. Available: <https://www.who.int/healthtopics/cardiovascular-diseases>
- [2] D.Boutana, M.Benidir, and B.Barkat, "Segmentation and Identification of Some Pathological Phonocardiogram Signals Using Time-Frequency Analysis," *IET Signal Processing*, vol. 5, no. 6, pp. 527-537, 2011. *Crossref*, <http://doi.org/10.1049/iet-spr.2010.0013>
- [3] João Pedrosa, Ana Castro, and Tiago T. V. Vinhoza, "Automatic Heart Sound Segmentation and Murmur Detection in Paediatric Phonocardiogram's," *Proceedings of Annual International Conference of the IEEE Engineering in Medicine and Biology Society*, Chicago, IL, pp. 2294-2297, 2014. *Crossref*, <http://doi.org/10.1109/EMBC.2014.6944078>
- [4] V. Nivitha Varghees, and K. I. Ramachandran, "Effective Heart Sound Segmentation and Murmur Classification Using Empirical Wavelet Transform and Instantaneous Phase for Electronic Stethoscope," *IEEE Sensors Journal*, vol. 17, no. 12, pp. 3861-3872, 2017. *Crossref*, <http://doi.org/10.1109/JSEN.2017.2694970>
- [5] Constantin Barabăsa, Maria Jafari, and Mark D. Plumley, "A Robust Method for S1/S2 Heart Sounds Detection Without ECG Reference Based on Music Beat Tracking," *Proceedings of 10th International Symposium on Electronics and Telecommunications*, Timisoara, pp. 307-310, 2012. *Crossref*, <http://doi.org/10.1109/ISETC.2012.6408110>

algorithm execution depends on the number of computations.

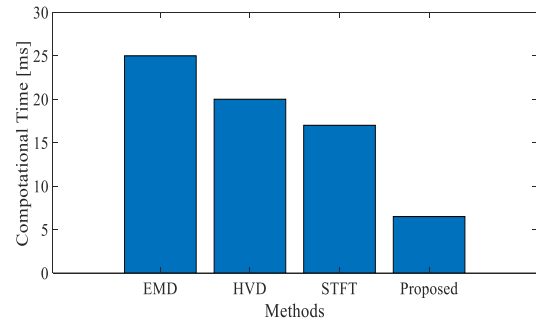


Fig. 13 Computational time compared with other methods.

The computational charge of the proposed workflow and other existing workflows are calculated. The methods are implemented in MATLAB on a personal computer with an Intel Core 2 Duo processor with 4GB RAM to determine the computational time. The obtained values are represented in Fig. 13, and further, it illustrates that the proposed method has achieved 6.5ms for processing a PCG signal of length 6s.

7. Conclusion

This paper discusses a technique for segmenting the first and second cardiac sounds using intrinsic time scale decomposition in conjunction with Shannon energy. Next, the locations of S1 and S2 are drawn from the proposed rules. The positional information of S1 and S2 are also inferred in the presence of S3 and S4. Further, the accuracy for 108 processed cardiac cycles is calculated and achieved at 95.2% for S1 and 90.5% for S2. Finally, the computational time of the proposed method is compared with the existing methods, revealing its effectiveness. The proposed method is contributed to the proper identification of cardiac sounds.

Author Contributions

Sai bharadwaj B wrote the paper with the obtained experimental results, Ch. Sumanth kumar designed and supervised the constructive procedure of the proposed work

- [6] Supreeya Swarup, and Amgad N Makaryus, "Digital Stethoscope: Technology Update," *Medical Devices (Auckl)*, vol. 11, pp. 29-36, 2018. *Crossref*, <http://doi.org/10.2147/MDER.S135882>
- [7] Hong Tang, Ting Li, and Tianshuang Qiu, "Cardiac Cycle Detection for Heart Sound Signal Based on Instantaneous Cycle Frequency," *Proceedings of 4th International Conference on Biomedical Engineering and Informatics (BMEI)*, Shanghai, pp. 676-679, 2011. *Crossref*, <http://doi.org/10.1109/BMEI.2011.6098371>
- [8] Sanmitra Banerjee, Madhusudhan Mishra, and Anirban Mukherjee, "Segmentation and Detection of First and Second Heart Sounds (S1 and S2) Using Variational Mode Decomposition," *Proceedings of IEEE EMBS Conference on Biomedical Engineering and Sciences (IECBES)*, Kuala Lumpur, pp. 565-570, 2016. *Crossref*, <http://doi.org/10.1109/IECBES.2016.7843513>
- [9] E Elmar Messner, Matthias Zöhrer, and Franz Pernkopf, "Heart Sound Segmentation—An Event Detection Approach Using Deep Recurrent Neural Networks," *IEEE Transactions on Biomedical Engineering*, vol. 65, no. 9, pp. 1964-1974, 2018. *Crossref*, <http://doi.org/10.1109/TBME.2018.2843258>
- [10] A Amit Krishna Dwivedi, Syed Anas Imtiaz, and Esther Rodriguez-Villegas, "Algorithms for Automatic Analysis and Classification of Heart Sounds—A Systematic Review," *IEEE Access*, vol. 7, pp. 8316-8345, 2019. *Crossref*, <http://doi.org/10.1109/ACCESS.2018.2889437>
- [11] Young Duck Shin et al., "The Correlation Between the First Heart Sound and Cardiac Output as Measured by Using Digital Esophageal Stethoscope Under Anaesthesia," *Pakistan Journal of Medical Sciences*, vol. 30, no. 2, pp. 276-281, 2014.
- [12] Dr. Vajed Mogal, and Dr. Sandeep Sanap, "Peripartum Cardiomyopathy: A Rare Case Report and a Brief Review of Literature," *SSRG International Journal of Medical Science*, vol. 7, no. 2, pp. 1-3, 2020. *Crossref*, <https://doi.org/10.14445/23939117/IJMS-V7I2P101>
- [13] Ali Moukadem et al., "A Robust Heart Sounds Segmentation Module Based on S-Transform," *Biomedical Signal Processing and Control*, vol. 8, no. 3, pp. 273–281, 2013. *Crossref*, <https://doi.org/10.1016/j.bspc.2012.11.008>
- [14] D. Kumar et al., "Third Heart Sound Detection Using Wavelet Transform-Simplicity Filter," in *Proceedings of 29th Annual International Conference of the IEEE Engineering in Medicine and Biology Society*, Lyon, pp. 1277-1281, 2007. *Crossref*, <https://doi.org/10.1109/IEMBS.2007.4352530>
- [15] Z. Sharif et al., "Analysis and Classification of Heart Sounds and Murmurs Based on the Instantaneous Energy and Frequency Estimations," *TENCON Proceedings Intelligent Systems and Technologies for the New Millennium*, Kuala Lumpur, Malaysia, vol. 2, pp. 130-134, 2000. *Crossref*, <https://doi.org/10.1109/TENCON.2000.888404>
- [16] Arash Gharehbaghi et al., "An Automatic Tool for Pediatric Heart Sounds Segmentation," in *Proceedings of Computing in Cardiology*, Hangzhou, pp. 37-40, 2011.
- [17] Mehak Saini, "Proposed Algorithm for Implementation of Shannon Energy Envelope for Heart Sound Analysis," *International Journal of Electronics & Communication Technology*, vol. 7, no. 1, pp. 15-19, 2016.
- [18] Runnan He et al., "Classification of Heart Sound Signals Based on AR Model," in *Proceedings of Computing in Cardiology Conference (CinC)*, Vancouver, BC, pp. 605-608, 2016. *Crossref*, <https://doi.org/10.22489/CinC.2016.177-133>
- [19] Noemi Giordano, and Marco Knaflitz, "A Novel Method for Measuring the Timing of Heart Sound Components through Digital Phonocardiography," *Sensors*, vol. 19, no. 8, p. 1868, 2019. *Crossref*, <https://doi.org/10.3390/s19081868>
- [20] Samjin Choi, and Zhongwei Jiang, "Comparison of Envelope Extraction Algorithms for Cardiac Sound Signal Segmentation," *Expert Systems with Applications*, vol. 34, no. 2, pp. 1056-1069, 2008. *Crossref*, <https://doi.org/10.1016/j.eswa.2006.12.015>
- [21] Ik-Soo Ahn, "A Study on Heart Management Using Healthy Heartbeat Frequency," *International Journal of Engineering Trends and Technology*, vol. 68, no. 12, pp. 16-21, 2020. *Crossref*, <https://doi.org/10.14445/22315381/IJETT-V68I12P203>
- [22] Samit Ari, and Goutam Saha, "Classification of Heart Sounds using Empirical Mode Decomposition Based Features," *International Journal of Medical Engineering and Informatics*, vol. 1, no. 1, pp. 91-108, 2008. *Crossref*, <https://doi.org/10.1504/ijmei.2008.019473>
- [23] H. Sharma, and K. K. Sharma, "Baseline Wander Removal of ECG Signals using Hilbert Vibration Decomposition," *In Electronics Letters*, vol. 51, no. 6, pp. 447-449, 2015. *Crossref*, <https://doi.org/10.1049/el.2014.4076>
- [24] P. S. Vikhe, N. S. Nehe, and V. R. Thool, "Heart Sound Abnormality Detection Using Short Time Fourier Transform and Continuous Wavelet Transform," in *Proceedings of Second International Conference on Emerging Trends in Engineering & Technology*, Nagpur, pp. 50-54, 2009. *Crossref*, <https://doi.org/10.1109/ICETET.2009.112>
- [25] Mark G Frei, and Ivan Osorio, "Intrinsic Time-Scale Decomposition: Time-Frequency-Energy Analysis and Real-Time Filtering of Non-Stationary Signals," *Proceedings of the Royal Society A: Mathematical, Physical and Engineering Sciences*, vol. 463, no. 2078, pp. 321–342, 2006. *Crossref*, <https://doi.org/10.1098/rspa.2006.1761>
- [26] Xinpei Wang et al., "Detection of the First and Second Heart Sound Using Heart Sound Energy," in *Proceedings of 2nd International Conference on Biomedical Engineering and Informatics*, Tianjin, pp. 1-4, 2009. *Crossref*, <https://doi.org/10.1109/BMEI.2009.5305640>
- [27] R. D. Judge and, R. Mangrulkar, "The Open Michigan Heart Sound & Murmur Library (OMHSML)," University of Michigan, 2015.
- [28] [Online]. Available: <https://depts.washington.edu/physdx/heart/demo.html>
- [29] Tien-En Chen et al., "S1 and S2 Heart Sound Recognition Using Deep Neural Networks," *IEEE Transactions on Biomedical Engineering*, vol. 64, no. 2, pp. 372-380, 2017. *Crossref*, <https://doi.org/10.1109/TBME.2016.2559800>